Supporting Information

Vapor-phase synthesis of low-valent metal-organic frameworks from metal carbonyl synthons

Carl Emil Andersen, James Neill McPherson, Mónica Giménez-Marqués, Jingguo Li, Mariusz Kubus, Sho Ito, Christian R. Göb, Sascha Ott, René Wugt Larsen, Guillermo Mínguez Espallargas, Kasper S. Pedersen

Journal of Materials Chemistry C

General Synthesis Considerations

All manipulations were carried out under a dry argon atmosphere in a glovebox unless otherwise stated. All chemicals are purchased from Sigma-Aldrich and used as received unless otherwise stated. All solvents were dried and deoxygenated on an Inert Technologies Solvent Purification System prior to use. The ITO coated glass substrates ($25 \times 25 \times 0.7$ mm^3, with an ITO coating of 140-150 nm) were acquired from Techinstro and cut in half before use. Silica glass substrates ($25 \times 25 \times 1$ mm^3) were cut in half prior to use.

Synthesis of W and Mo

Ampoule Reactions:

W: Two oven-dried glass ampoules (V = 21 mL) were each charged with $W(CO)_6$ (68.7 mg, 0.195 mmol) and 4,4′-bipyridine (305 mg, 1.95 mmol) and sealed under vacuum. The sealed ampoules were shaken extensively and placed horizontally in a muffle furnace with the powder mixture evenly distributed. The ampoules were heated to 240 °C over 4 h, then held at this temperature for 40 h before they were cooled to room temperature over 16 h. The black microcrystalline products were combined and washed with acetonitrile (50 mL), collected by filtration, and dried under a dynamic vacuum. To further remove pore-contained 4,4′-bipyridine, the crystalline powder was ground and soaked in acetonitrile overnight, filtered, and dried under a dynamic vacuum. Phase pure **W** was identified by powder X-ray diffraction (Fig. 3a). Yield: 57 mg (29%, based on W). ATR-FTIR: $\tilde{\upsilon}$ = 1756 cm^{-1} (vs), 1880 cm^{-1} (vs) (C≡O); calculated (found) elemental analysis for $WC_{18}O_3N_3H_{12}$: C 43.05% (42.95%), N 8.37% (8.34%), H 2.41% (2.43%), W 36.61% (36.47%).

Mo: The synthesis proceeded similarly to that of **W**, using $Mo(CO)_6$ (110 mg, 0.417 mmol) and 4,4′-bipyridine (450 mg, 2.88 mmol), and a maximum temperature of 200 °C in contrast to 240 °C for **W**. The initially washed product was analytically freed of pore-occupying bipy and phase pure **Mo** could be identified by powder X-ray diffraction (Fig. S10). Yield: 113 mg (65%, based on Mo). ATR-FTIR: $\tilde{\upsilon}$ = 1765 cm^{-1} (vs), 1893 cm^{-1} (vs) (C≡O); calculated (found) elemental analysis for $MoC_{18}O_3N_3H_{12}$: C 52.19% (51.95%), N 10.14% (10.18%), H 2.92% (2.97%), Mo 23.16% (22.73%). **Mo** was activated by washing microcrystalline samples with tetrahydrofuran or dichloromethane followed by soaking in the same solvent for 24 h, followed by filtration. The samples were then dried under vacuum at 70 °C overnight to remove any remaining solvent guests. The diffractograms before and after activation are shown in Fig. S11. The samples were further activated by heating at 100 °C under a dynamic vacuum prior to CO_2 gas sorption analysis (Fig. S12).

One-dimensional, polymeric $M(CO)_3(bipy)_2$ networks (**Mo***, **W***) were persistent impurities found from non-optimized synthesis conditions, and their structures determined from SC-XRD (**W***) or 3D-ED (**Mo***) data (see Fig. S8). The synthetic protocols were optimized to avoid any detectable formation of these compounds.

Vapor-Phase Synthesis of W and Mo

W (glass), **W** (ITO): $W(CO)_6$ (133 mg, 0.378 mmol) and 4,4′-bipyridine (600 mg, 3.84 mmol) were loaded in separate glass vials (12 mL) and placed in a 100 mL Teflon beaker containing two plates of the chosen substrate (glass or ITO on glass, *vide supra*) fixed to the inside of the lid with brass thumb tacks. The Teflon beaker was inserted into a hydrothermal autoclave reactor which was then heated to 240 °C over 1 h and held at that temperature for 4 h. The autoclave assembly was then removed from the oven and allowed to cool down to room temperature overnight in an antechamber under vacuum. After transferring into an argon filled glovebox, the substrate plates were removed and examined as described in the main text.

Mo (glass), **Mo** (ITO): The **Mo** substrate coatings were prepared as above, but the procedure utilized $Mo(CO)_6$ (100 mg, 0.379 mmol) and 4,4′-bipyridine (600 mg, 3.84 mmol), and a maximum heating temperature of 200 °C. The substrate specimens were as described above. To elucidate the influence of the thermal treatment on the crystallinity of the coatings on the substrate, an identical experiment was performed by inserting the reactor in a pre-heated muffle furnace at 200 °C and kept for 2 h before being removed from the furnace. A black powder could be isolated from the Teflon coated vessel, mainly from the 4,4′-bipyridine-vial, and soaked in tetrahydrofuran overnight. The black microcrystalline powder was collected by filtration and washed with 3 × 2 mL tetrahydrofuran and 3 × 2 mL acetonitrile before being subjected to dynamic vacuum overnight at 70 °C. The black powder was identified as **Mo** by powder X-ray diffraction. Yield: 91 mg. Calculated (found) elemental analysis for $MoC_{18}O_3N_3H_{12}·0.15(N_2C_{10}H_8)$: C 53.51% (53.89%), N 10.56% (10.59%), H 3.04% (3.35%).

Synthesis of Reference Compound

***fac*-Mo(CO)$_3$(pyridine)$_3$**: *fac*-$Mo(CO)_3(pyridine)_3$ was obtained from a modified literature procedure:[1] a 25 mL Schlenk flask was charged with $Mo(CO)_6$ (1.87 g, 7.08 mmol) and pyridine (10 mL). The mixture was immediately heated to reflux and left for 2.5 h before being allowed to cool down to room temperature overnight. To the dark red solution, with a significant amount of yellow-orange precipitate, was added heptane (10 mL), whereafter it was cooled in an ice bath for 20 min. The yellow-orange crystalline product was filtered under ambient atmosphere, and washed with 3 × 10 mL heptane and 3 × 10 mL diethyl ether, and dried *in vacuo* for 1 h. Phase-pure *fac*-$Mo(CO)_3(pyridine)_3$ was identified by powder X-ray diffraction (Fig. S14) and elemental analysis. Yield = 2.30 g (77.8%). Calculated (found) elemental analysis for $MoC_{18}O_3N_3H_{15}$: C 51.81% (51.65%), N 10.07% (10.04%), H 3.62% (3.68%).

Instrumentation, Analysis, and Modelling

Powder X-Ray Diffraction: All powder X-ray diffraction experiments (except for activated **Mo**, *vide infra*) were conducted on a Malvern Panalytical Empyrean diffractometer, equipped with a 1Der detector, using Cu Kα (λ = 1.5406 Å) radiation in reflection mode at a voltage of 45 kV and a current of 40 mA. Bulk samples were measured at room temperature on a reflection/transmission spinner between 2θ = 4–50° with a step size of 0.008° at a scan speed of 0.08° s^{-1}. Coatings were measured using an Anton Paar TTK 600 non-ambient chamber and a dry argon atmosphere at room temperature between 4–50° with a step size of 0.008° at a scan speed of 0.001° s^{-1}. The sample height was corrected prior to measuring such that the first intense peak of **W** (*hkl* = 2,0,0) and **Mo** (*hkl* = 0,2,0) were aligned at 2θ = 10.64°. Powder X-ray diffraction data of activated **Mo** was recorded using 0.7 mm borosilicate capillaries that were aligned on an Empyrean PANalytical powder diffractometer, using Cu Kα (λ = 1.5406 Å), with a PIXcel detector.

Single-Crystal X-Ray Diffraction: Single-crystals of **Mo** and **W*** were collected directly from the crude ampoule reaction mixture, suspended in polybutenes and mounted on a loop onto a Supernova DualSource diffractometer. Experiments were conducted in a nitrogen stream at 120 K using Cu Kα radiation. The structures were solved with ShelXT[2] using intrinsic phasing and refined by least squares with ShelXL[3] using Olex2.[4] The **Mo** crystal was twinned with a twin ratio below 10%. Because of strongly overlapping diffraction patterns, the structure was refined as a single-crystal. Attempts to solve **Mo** in the monoclinic $P2/c$ space group were unsatisfactory, and so the triclinic $P\bar{1}$ space group was used instead. A rigid body restraint (RIGU) was used to keep anisotropic displacement parameters (ADPs) stable during refinement. Positional disorder in one of the bridging 4,4′-bipyridine ligands could be partially modelled (freely refined to 60%:40% occupancy), with SADI restraints to keep N—C, C—C, and 1,3-N···C and -C···C atomic separations similar across the two disordered positions. Three positionally disordered, unbound 4,4′-bipyridine residues were located at partial occupancies (each refined freely to 62%, 61%, and 36%) in the pores of the interpenetrated $Mo(CO)_3(bipy)_{3/2}$ networks. The N—C bonds were restrained to 1.34 Å in all three residues, as were the intra-ring C—C bonds to 1.38 Å. The 1,3-N···C and intra-ring 1,3-C···C interatomic separations were similarly restrained to 2.4 Å using the DANG instruction. FLAT restraints were used for the six atoms in each pyridyl ring, and a second set of FLAT instructions were used to ensure the inter-ring C_{ipso} atoms remained planar. SIMU and ISOR restraints were also used to keep the ADPs of the atoms in the disordered, unbound 4,4′-bipyridine residues stable during refinement. All restraints were used with default standard deviations. The **W*** crystal was twinned with a BASF parameter of 39%.

3D Electron Diffraction: Continuous rotation 3D electron diffraction data were acquired using the dedicated electron diffractometer Rigaku XtaLAB Synergy-ED, equipped with a HyPix-ED detector by Rigaku Oxford Diffraction[5]. Data acquisition was performed at ambient temperature with an electron wavelength of 0.0251 Å (200 kV). The data were processed using CrysAlis^{Pro},[6] the structure was solved using ShelXT[2] and subsequently refined using the kinematical approximation in ShelXL[3] in the crystallographic program suite Olex2.[4] By merging the data of two individual crystals, a completeness of 86.3% up to a resolution of 0.98 Å was achieved for **Mo*** and a completeness of 80.5% at 0.80 Å resolution for **W**. The crystals screened for the diffraction analysis can be seen in Fig. S1 and Fig. S2 for **W** and **Mo***, respectively.

Scanning Electron Microscopy: Scanning electron microscopy images were measured on an AFEG 250 Analytical ESEM and generated with secondary electrons detected by Everhart-Thornley detector at the following settings: high tension = 2 kV (**Mo** (glass)) or 5 kV (all other coatings), spot size = 3.5, working distance = 10.0 mm. All MOF-coatings were coated with 3-6 nm Au prior to imaging and held in place by conductive copper- and carbon tape.

Infra-Red Spectroscopy: The attenuated-total-reflectance (ATR) Fourier Transform infrared (FTIR) spectra shown in Fig. 3b, Fig. S16 and Fig. S17 were obtained by a VERTEX80v FTIR vacuum spectrometer (Bruker Optics, GmbH) employing a single reflection germanium (for Fig. 3b and Fig. S17) ATR accessory (PIKE Technologies Inc) or a single reflection diamond ATR accessory (Fig. S16). The FTIR apparatus was equipped with a Ge/KBr beam splitter and a liquid nitrogen cooled MCT (HgCdTe) detector in combination with an air-cooled silicon carbide thermal radiation source. The obtained ATR spectra of 2 cm^{-1} spectral resolution have been corrected for residual gas-phase water absorption. The resulting absorbance spectra have subsequently been corrected for minor drifts of the baseline before extended ATR corrections were applied to account for the wavelength-dependent penetration depth of the probe beam.

Gas Adsorption Analysis: CO_2 sorption isotherms were obtained using a TRISTAR II apparatus (Micromeritics) at 273 K. A powder sample of **Mo** was activated overnight at 100 °C under a dynamic vacuum before the measurement, as described above.

Thermogravimetric Analysis: TGA were conducted on a Thermogravimetric Analyzer from Mettler-Toledo. Approximately 10 mg of sample was used per analysis, which were all performed under a flow of dry Ar.

Elemental Analysis: Elemental analysis of C, H, N, Mo, and W content was conducted by Microanalytisches Laboratorium Kolbe (Oberhausen, Germany). The samples were handled under a dry argon atmosphere and all analyses performed in duplicates. The percentages for the elemental composition are given as the average of the measurements. Elemental analysis of C, H, N content was conducted on a Thermo Scientific FlashSmart Elemental Analyzer. The samples were handled in ambient atmosphere and all analyses were performed in triplicates. The percentages for the elemental composition are given as the average of the measurements.

Electrochemical Analysis: Cyclic voltammetry was measured in a electrochemical cell with the ITO or coated ITO as working electrodes and measured against a AgCl/Ag reference. Reference drift was corrected against Fc^+/Fc at the end of measurements. The electrochemistry was conducted in 0.1 M $LiClO_4$ in dimethylformamide electrolyte solution under Ar atmosphere and protected from light irradiation, with the scan rate specified at the results. The coated ITO working electrodes were made with a slightly modified method from the one described in the experimental section; ITO substrates was cut into appr. 1 cm × 1cm before covering half of the substrate with tightly with aluminium foil. The substrates were then attached as described earlier in a Teflon beaker containing $Mo(CO)_6$ (100 mg) and 4,4′-bipyridine (600 mg), before being heated to 200 °C over 1 h, held there for 4 h, and cooled to room-temperature in an antechamber overnight. The aluminium foil was carefully removed prior to analysis.

Table S1. 3D electron diffraction data for **W** and **Mo***.

	W	**Mo***
CCDC Code	2233879	2233877
Empirical Formula	$W(CO)_3(C_{10}H_8N_2)_{3/2}$	$Mo(CO)_3(C_{10}H_8N_2)_2$
Merged Datasets	2	2
Scan Width (° frame^{-1})	0.25 / 0.25	0.25 / 0.25
Scan Range (°)	−60 to +60 / −60 to +60	−60 to +60 / −60 to +60
Space Group	$P2/c$ (13)	$P2_1/c$ (14)
a, b, c (Å)	16.8(2), 32.54(8), 7.49(10)	16.30(13), 36.6(2), 7.82(14)
α, β, γ (°)	90, 92.86(12), 90	90, 94.16(18), 90
Resolution (Å)	0.80	1.00
Independent Reflections	6782	4215
Completeness (%)	80.9	86.6
$I / \sigma(I)$	8.5	6.6
R_1 (%)	23.52	20.14
R_{int} (%)	20.14	30.65
R_{pim} (%)	10.10	13.50

Table S2. Single-crystal X-ray diffraction data for **W*** and **Mo**.

	W*	**Mo**
CCDC Code	2233878	2233880
Empirical formula	$W(CO)_3(C_{10}H_8N_2)_2$•$0.175(C_{10}H_8N_2)$,$0.5H_2O$	$Mo(CO)_3(C_{10}H_8N_2)_{3/2}$•$0.437(C_{10}H_8N_2)$
Formula weight	616.59	474.77
Temperature (K)	120.0	120.0
Crystal system	monoclinic	triclinic
Space group	$P2_1/c$ (14)	P–1 (2)
a (Å)	16.32077(18)	7.49470(12)
b (Å)	36.0142(4)	16.6511(4)
c (Å)	7.65607(8)	32.5041(6)
α (°)	90	93.2185(16)
β (°)	96.0574(9)	90.5015(13)
γ (°)	90	92.2033(15)
Volume (Å^3)	4474.96(8)	4046.71(13)
Z	8	8
ρ_{calc} (g cm^{-3})	1.830	1.559
μ (mm^{-1})	9.896	5.563
$F(000)$	2395.0	1910.0
Crystal size (mm^3)	0.198 × 0.051 × 0.012	0.47 × 0.06 × 0.05
Radiation	Cu Kα (λ = 1.54184 Å)	Cu Kα (λ = 1.54184 Å)
2θ range (°)	7.332 to 153.316	7.398 to 153.616
Index ranges	$-20 \le h \le 20$, $-45 \le k \le 45$, $-9 \le l \le 6$	$-9 \le h \le 7$, $-20 \le k \le 21$, $-40 \le l \le 40$
Reflections collected	24475	51074
Independent reflections	24475 [R_{sigma} = 0.0361]	16778 [R_{int} = 0.0679, R_{sigma} = 0.0598]
Data/restraints/parameters	24475/255/668	16778/1675/1244
Goodness-of-fit on F^2	1.057	1.073
Final R indexes [$I \geq 2\sigma(I)$]	R_1 = 0.0439, wR_2 = 0.1167	R_1 = 0.1161, wR_2 = 0.3021
Final R indexes [all data]	R_1 = 0.0588, wR_2 = 0.1236	R_1 = 0.1297, wR_2 = 0.3130
Largest diff. peak/hole (e Å^{-3})	1.46/–1.01	1.81/–1.48

Table S3. Metric data from 3D-ED and SC-XRD structures of **W** and **Mo**.

	W		**Mo**			
	W01	W02	Mo1	Mo2	Mo3	Mo4
M–N / Å	2.31(2)	2.33(2)	2.326(9)	2.32(1)	2.32(1)	2.30(1)
M–N / Å	2.29(2)	2.30(2)	2.29(1)	2.29(1)	2.29(1)	2.293(9)
M–N / Å	2.30(1)	2.30(2)	2.29(1)	2.29(1)	2.32(1)	2.33(1)
M–C / Å	1.97(2)	1.97(3)	1.95(2)	1.95(2)	1.95(2)	1.96(1)
M–C / Å	2.00(3)	1.89(2)	1.93(1)	1.93(2)	1.94(1)	1.96(2)
M–C / Å	1.98(2)	1.88(3)	1.95(2)	1.94(2)	1.97(1)	1.92(2)
<M–N>$_{av}$ / Å	2.30	2.31	2.30	2.30	2.31	2.31
	2.31 (2.29–2.33)		2.30 (2.29–2.33)			
<M–C>$_{av}$ / Å	1.98	1.91	1.94	1.94	1.95	1.95
	1.95 (1.88–2.00)		1.95 (1.92–1.97)			
C–O / Å	1.06(3)	1.09(4)	1.15(2)	1.14(2)	1.14(2)	1.14(2)
C–O / Å	1.10(4)	1.18(3)	1.15(2)	1.13(2)	1.17(2)	1.17(2)
C–O / Å	1.12(3)	1.15(5)	1.19(2)	1.16(2)	1.17(2)	1.17(2)
<C–O>$_{av}$ / Å	1.09	1.14	1.16	1.14	1.16	1.16
	1.12 (1.06–1.18)		1.16 (1.13–1.19)			
N1–M–N2 / °	93.1(3)	92.1(4)	91.6(4)	87.0(4)	90.1(4)	89.0(3)
N1–M–N3 / °	86.3(3)	91.7(4)	89.0(3)	93.5(4)	87.9(4)	92.0(3)
N2–M–N3 / °	82.0(4)	78.2(4)	81.8(4)	80.3(4)	82.2(4)	80.3(4)
N1–M–C2 / °	86.3(6)	94.2(7)	90.2(5)	94.6(5)	88.2(5)	90.6(6)
N1–M–C3 / °	94.4(6)	88.7(7)	90.6(5)	89.0(5)	92.4(5)	92.3(6)
N2–M–C1 / °	92.4(6)	93.9(7)	81.8(4)	93.7(6)	94.9(5)	92.2(4)
N2–M–C3 / °	91.6(6)	97.5(8)	95.1(6)	101.1(6)	91.5(5)	97.6(6)
N3–M–C1 / °	92.8(6)	91.2(7)	95.6(5)	92.6(6)	91.0(5)	86.6(6)
N3–M–C2 / °	98.4(6)	99.6(7)	93.0(6)	93.1(6)	101.6(5)	83.9(8)
C1–M–C2 / °	88.2(8)	79.8(9)	87.6(7)	84.9(7)	87.0(6)	84.0(6)
C1–M–C3 / °	87.0(8)	88.7(9)	83.1(7)	85.4(7)	89.4(6)	86.6(6)
C2–M–C3 / °	88.0(8)	85(1)	83.4(6)	85.5(7)	84.6(6)	83.9(8)
cis-<L–M–L>$_{av}$ / °	90.0	90.1	88.6	90.1	83.2	88.3
	90.0 (78.2–99.6)		89.0 (80.3–101.6)			
Angle variance / °^{2}	20.3	42.0	25.2	32.6	29.0	24.0

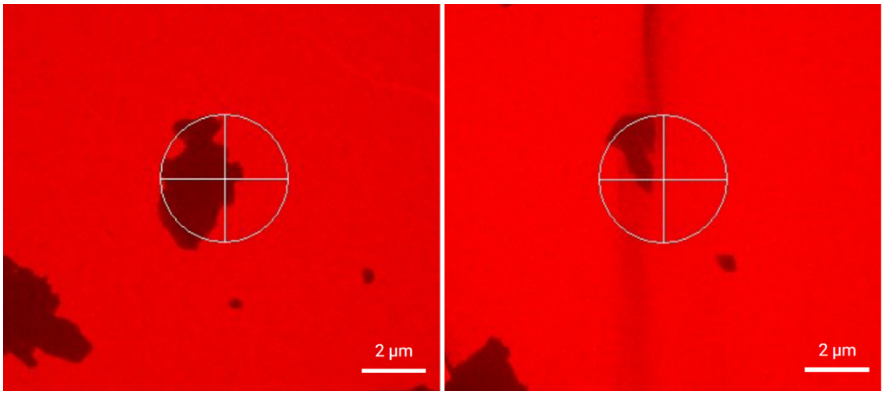

Fig. S1. Crystals used for 3D-ED analysis, leading to the structural elucidation of **W**.

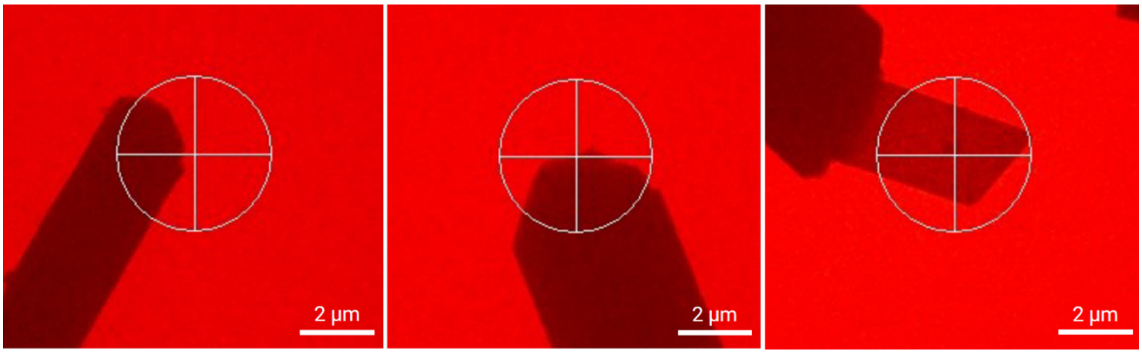

Fig. S2. Crystals screened for 3D-ED analysis for the structural elucidation of **Mo***.

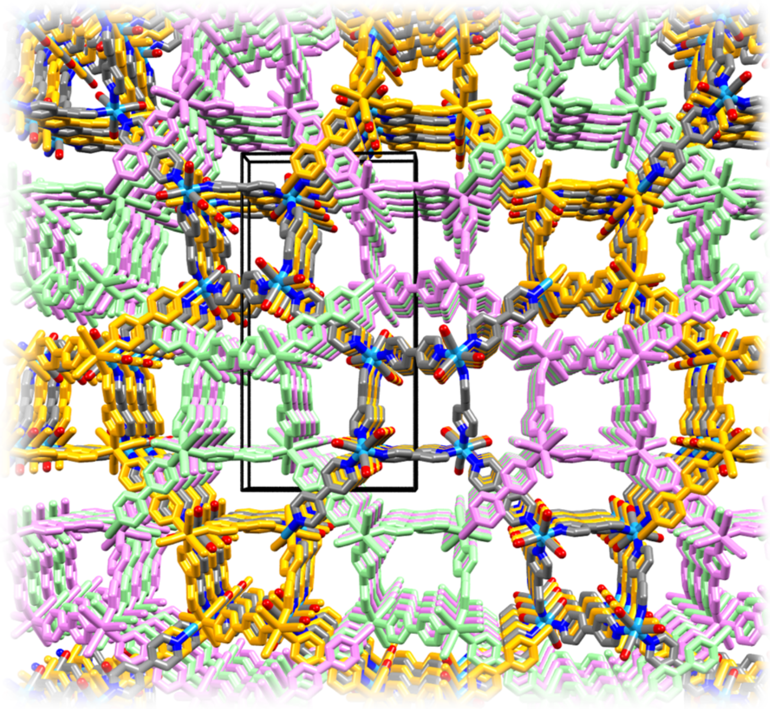

Fig. S3. 3D-ED structure of **W** as viewed down the crystallographic *c* axis illustrating the interpenetrated network architecture, with one network colored by atom type, and each other network colored either orange, green or violet. Color codes: W, light blue, C, grey; O, red; N blue. H-atoms are omitted for clarity.

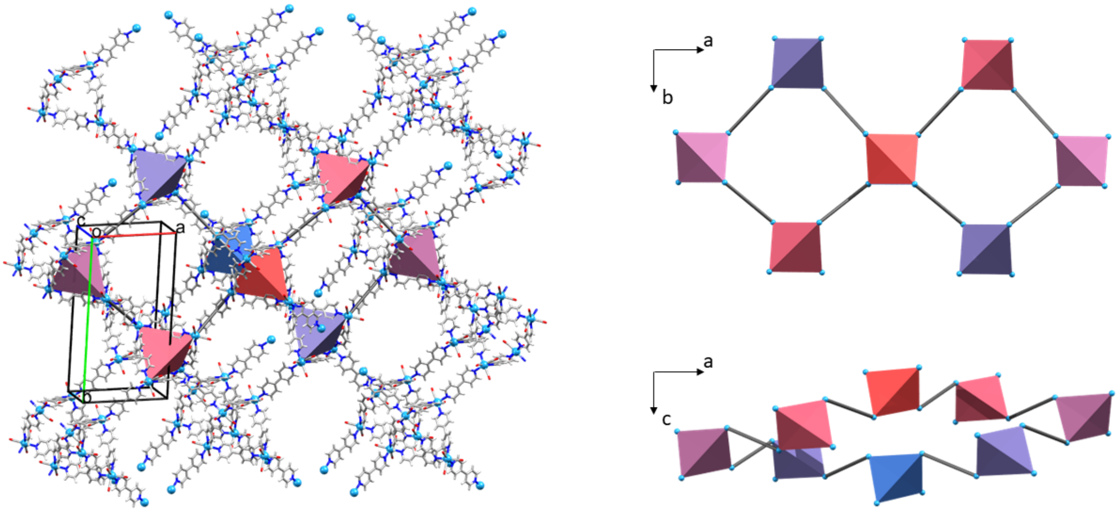

Fig. S4. Extended 3D-ED structure of one of the four interpenetrated **W** networks, with the tetrahedral SBUs for one ‘topological loop’ depicted and extracted on the right viewed either along the *c* axis (top right) or *b* axis (bottom right).

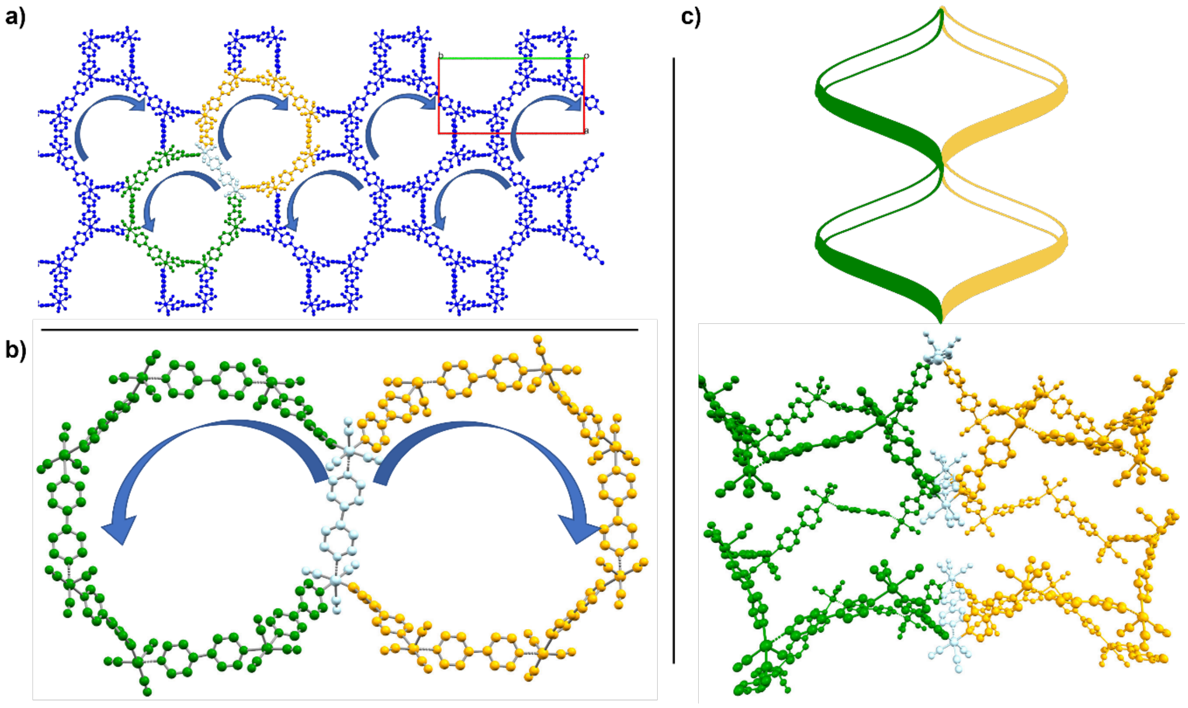

Fig. S5. 3D-ED structure of **W**. **a)** Illustration of a single framework in **W**. Two connecting octagonal staircases are highlighted in green and yellow sharing one W(CO)$_3$–bipy–W(CO)$_3$ “ledge” (light blue). **b)** Two connected octagonal staircases (green and yellow) with light blue sharing “ledge”. The two spirals are turned 90° in **c)**, where the green and yellow spirals above mimic the turning of the green and yellow network respectively.

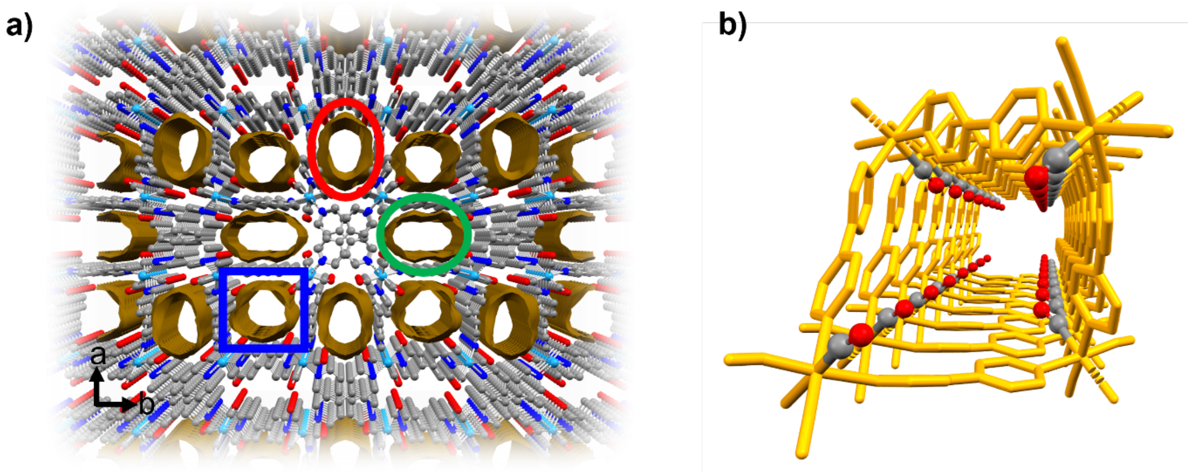

Fig. S6. **a**) 3D-ED structure of **W**, highlighting the three crystallographically different pores (blue square, green – and red circles), with **b**) illustrating the accessibility of the carbonyls in the blue square pore.

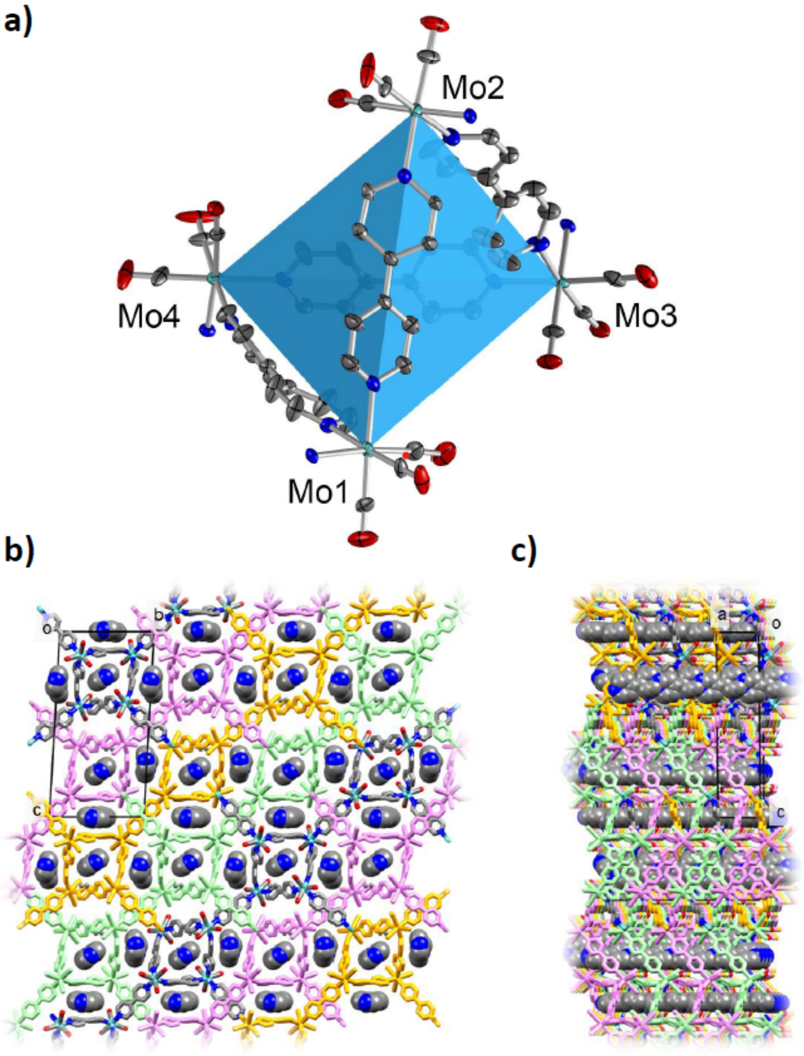

Fig. S7. a) 120 K SC-XRD structure of the tetrahedral SBU, $\{Mo(CO)_3(bipy)\}_4$, of **Mo**, showing the thermal ellipsoids at 30% probability level. The coordination sphere is completed by half a bipy for each Mo center (with the N atom depicted). **b/c)** SC-XRD structure of **Mo**. Two views of the crystal structure of **Mo** as viewed down the crystallographic *a*-axis (**b**) or *b*-axis (**c**), illustrating the interpenetration of the networks. For clarity, one framework is represented by sticks colored by element type, and its corresponding 'double threaded' network represented by orange sticks. The remaining two interpenetrated networks are represented with green or pink ball-and-sticks. The bipy guest-molecules are represented by their elemental colors. Unbound bipy guests are represented by spacefills colored by element type. Color code: Mo, light green; C, grey; O, red; N blue. H atoms have been omitted for clarity.

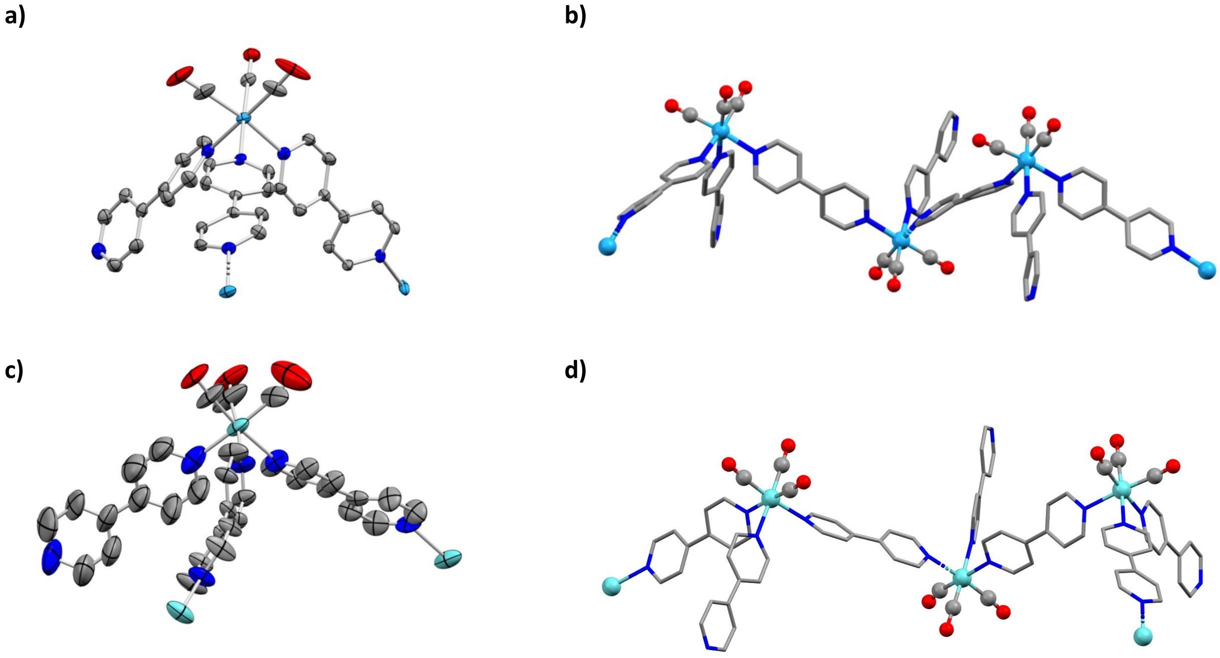

Fig. S8. SC-XRD structure (**a**, **b**) of **W*** and 3D-ED structure (**c**, **d**) of **Mo***. The ellipsoids (**a**, **c**) are shown at 50% probability level. Panels **b** and **d** depict the one-dimensional nature. Color code: W, light blue; Mo, light green; C, grey; O, red; N blue. H atoms have been omitted for clarity.

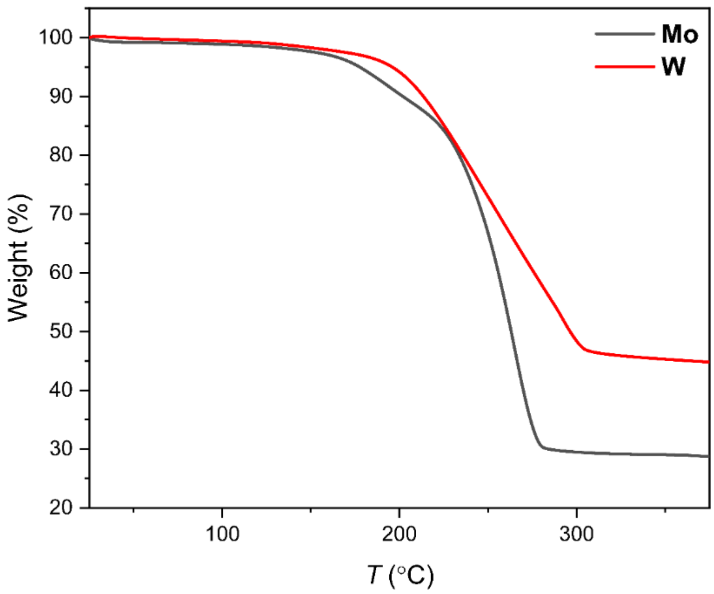

Fig. S9. TGA of bulk **Mo** and **W**. The samples were heated at 1 °C min^{-1} from 25 to 375 °C in a dry Ar atmosphere.

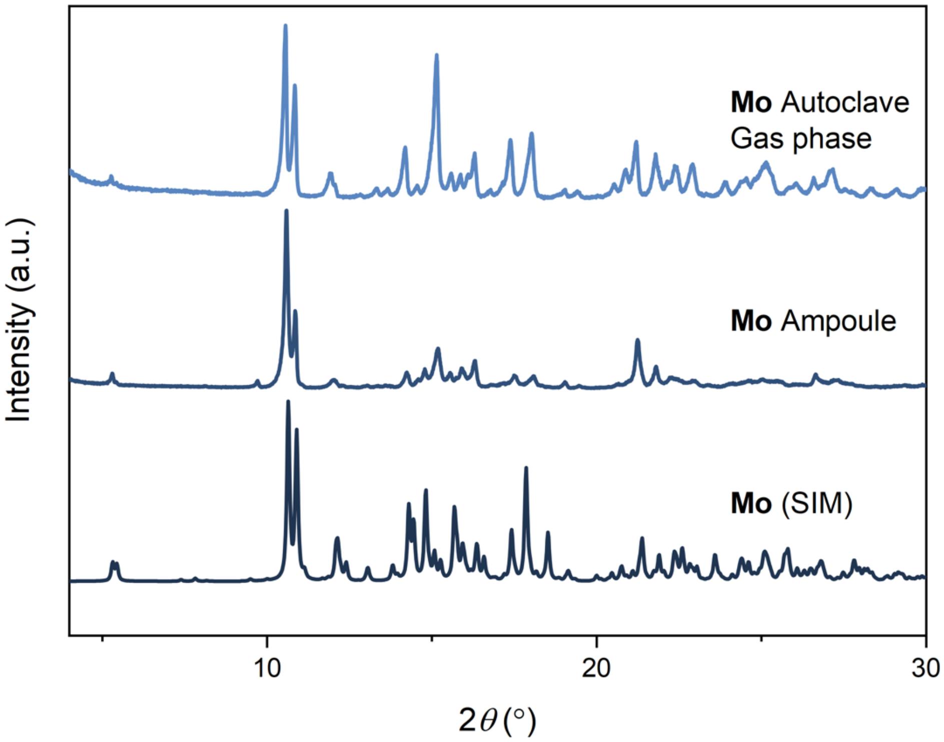

Fig. S10. Powder X-ray diffractograms (Cu Kα, λ = 1.5406 Å) of **Mo** synthesized from different methods.

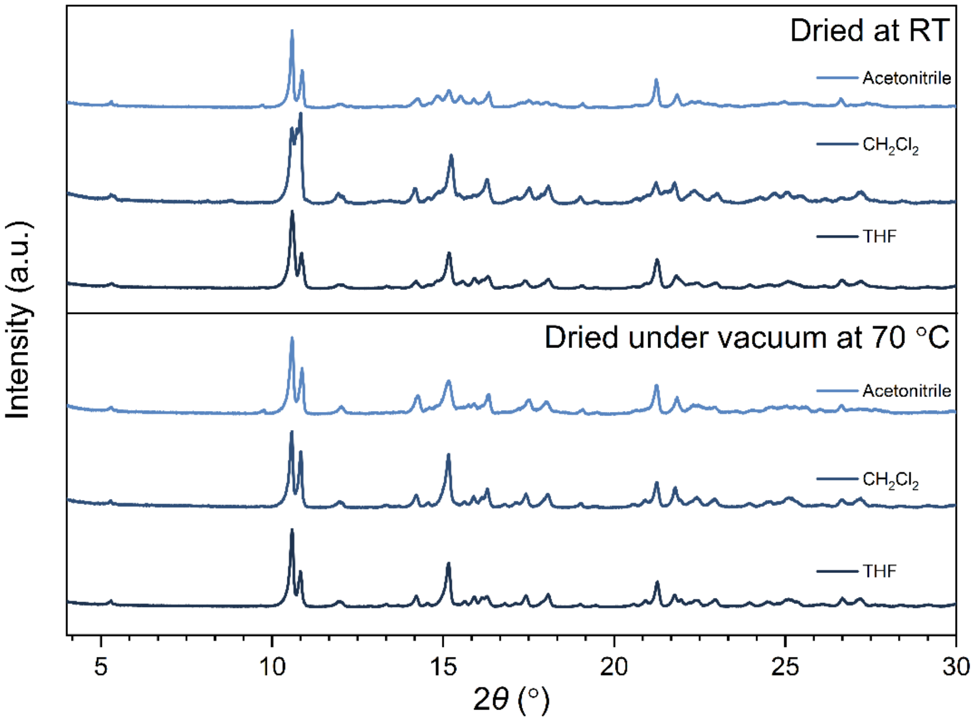

Fig. S11. Powder X-ray diffractograms (Cu Kα, λ = 1.5406 Å) of **Mo** either washed with acetonitrile, THF, or dichloromethane (soaked for 24 hours, bottom) before (top) and after (bottom) drying under a dynamic vacuum at 70 °C overnight.

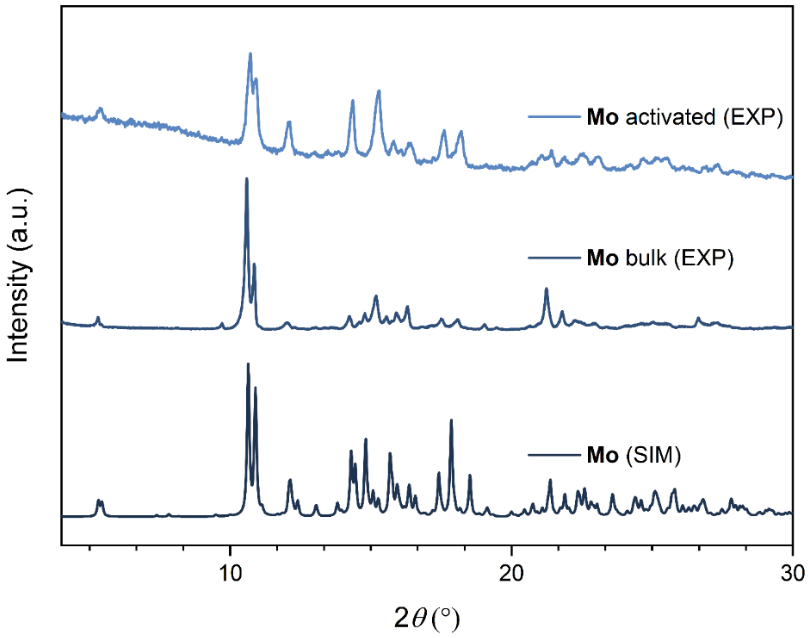

Fig. S12. Powder X-ray diffractograms (Cu Kα, λ = 1.5406 Å) of **Mo** before and after activation overnight under vacuum at 100 °C.

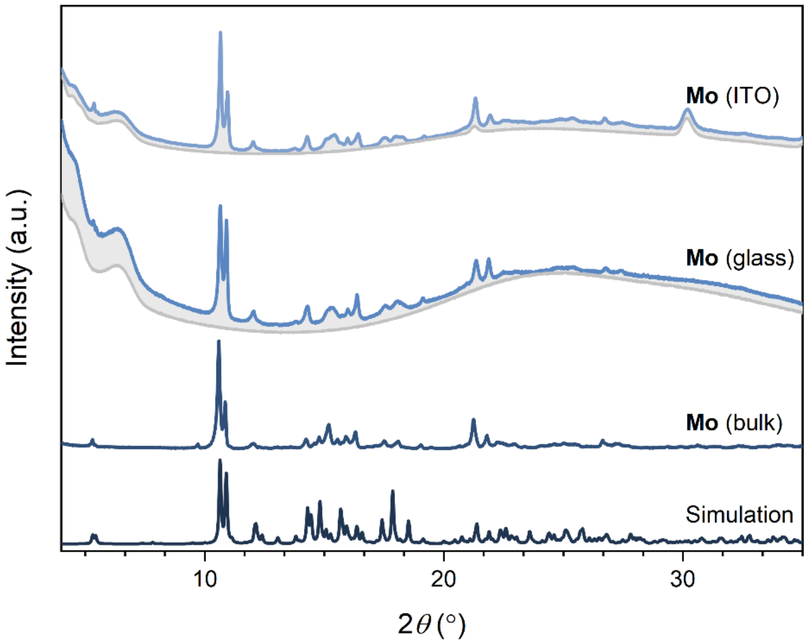

Fig. S13. Powder X-ray diffractograms (Cu Kα, λ = 1.5406 Å) of **Mo** (ITO) and **Mo** (glass) (blue traces, with grey traces representing uncoated substrate backgrounds), compared with an experimental diffractogram from the product of bulk gas-phase synthesis, as well as a simulated diffractogram.

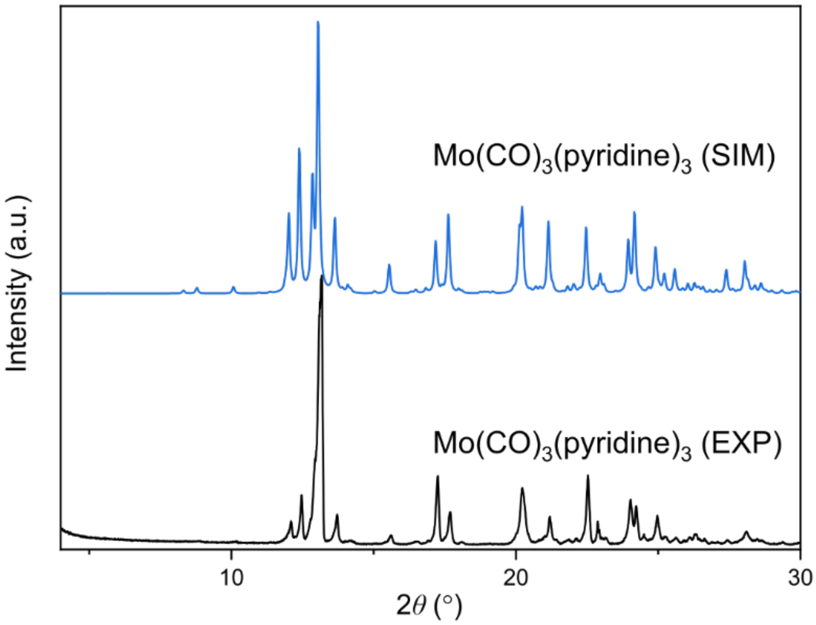

Fig. S14. Powder X-ray diffractogram (Cu Kα, λ = 1.5406 Å) of $Mo(CO)_3(pyridine)_3$.

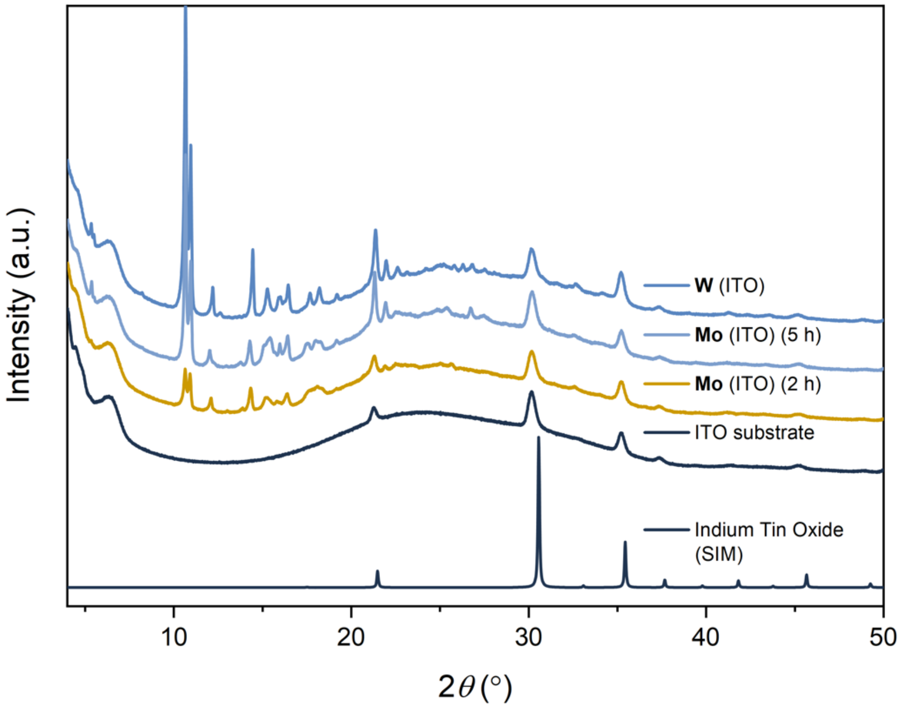

Fig. S15. Powder X-ray diffractograms (Cu Kα, λ = 1.5406 Å) of **W** (ITO) and **Mo** (ITO) substrates together with uncoated ITO substrate and a simulated diffractogram of ITO (ICSD-50848)[7].

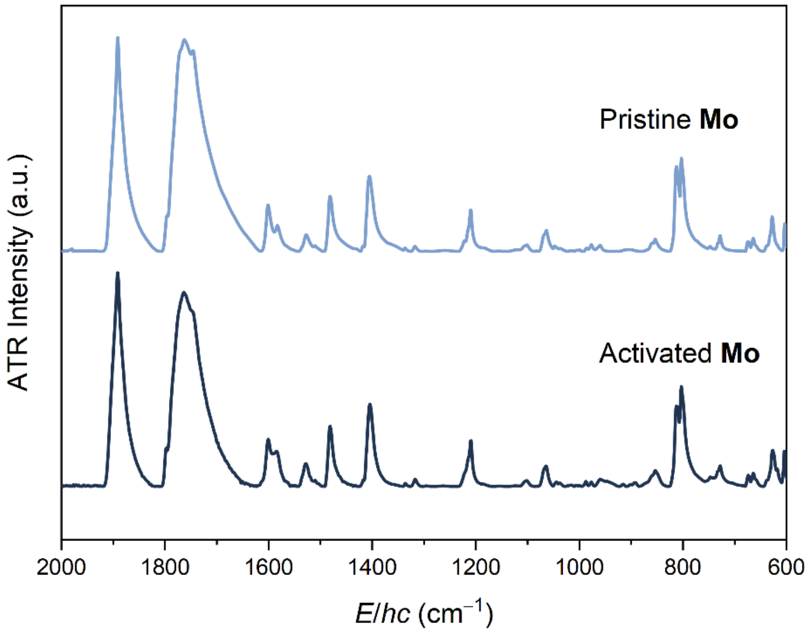

Fig. S16. ATR-FTIR spectra of activated **Mo** compared with the non-activated bulk material.

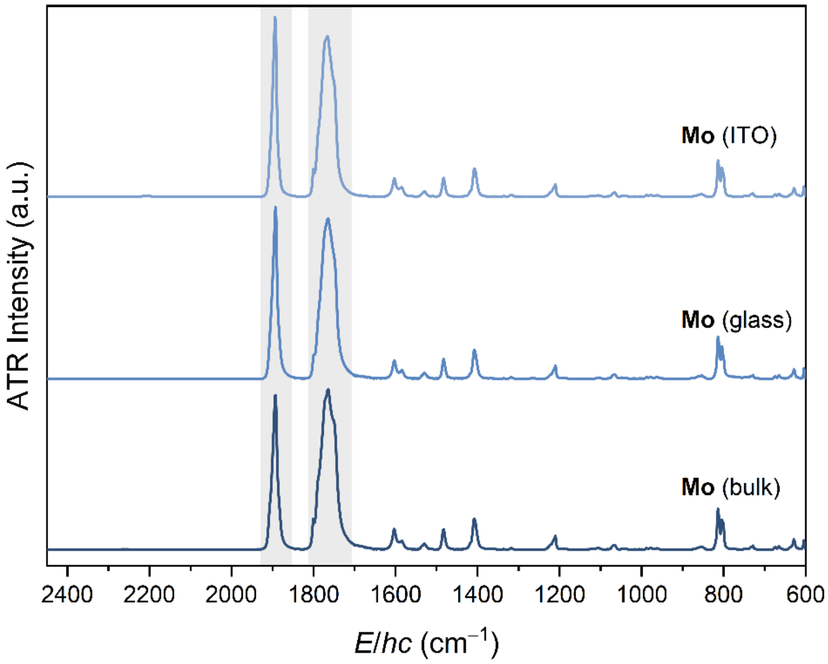

Fig. S17. ATR-FTIR spectra of **Mo** (ITO) and **Mo** (glass), compared with the experimental spectrum collected on the bulk material.

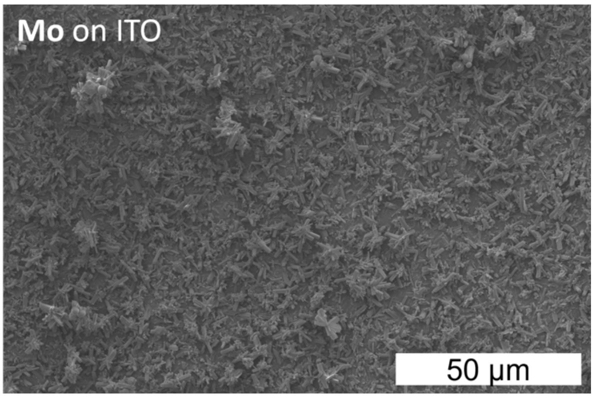

Fig. S18. Scanning electron microscopy generated image of **Mo** (ITO) prepared by 5 h reaction time (see Synthesis section).

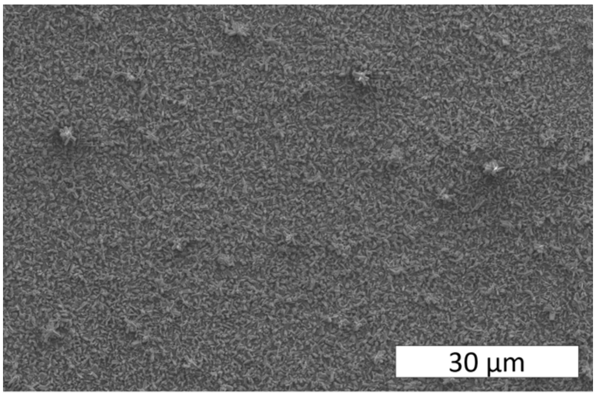

Fig. S19. Scanning electron microscopy generated image of **Mo** (ITO) prepared by 2 h reaction time (see Synthesis section).

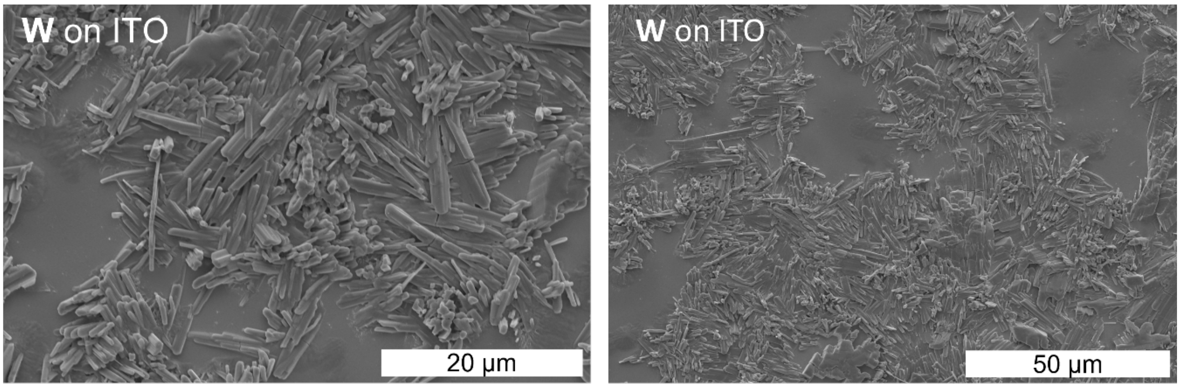

Fig. S20. Scanning electron microscopy generated image of **W** (ITO) at different magnifications.

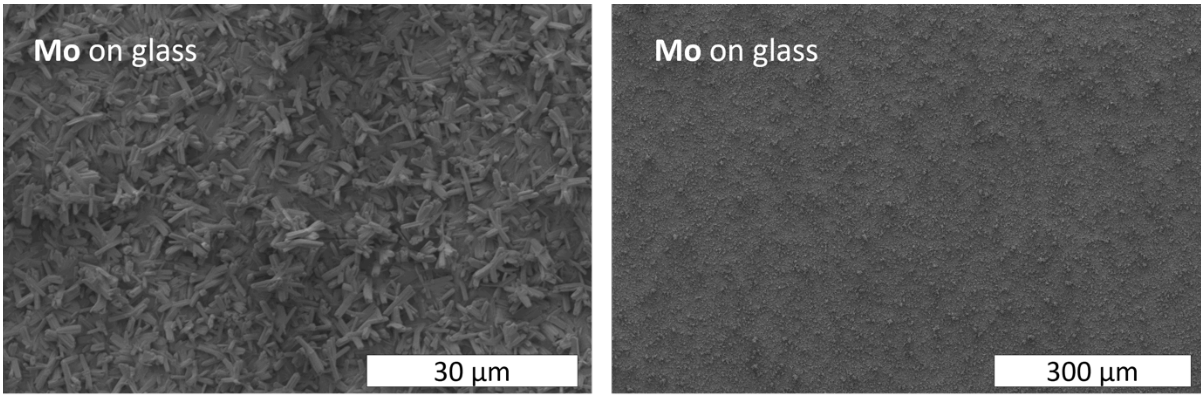

Fig. S21. Scanning electron microscopy generated image of **Mo** (glass) at different magnifications.

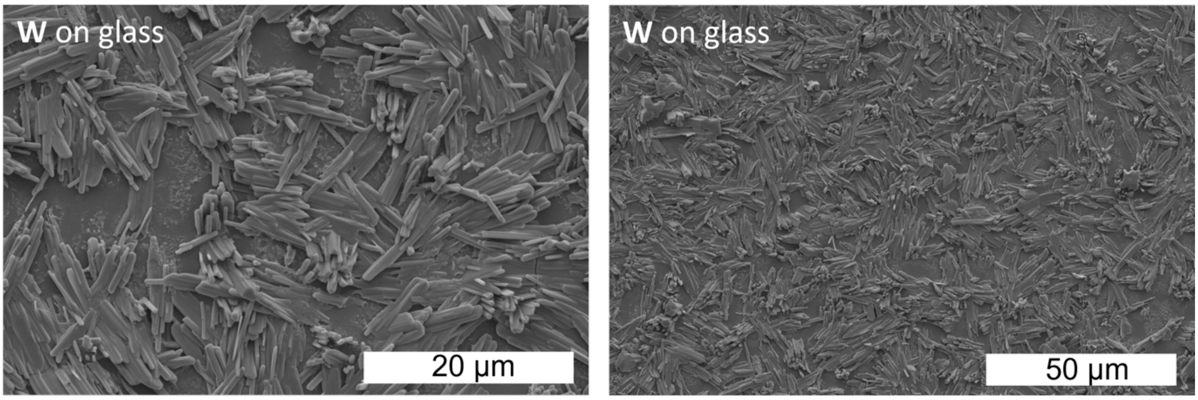

Fig. S22. Scanning electron microscopy generated image of **W** (glass) at different magnifications.

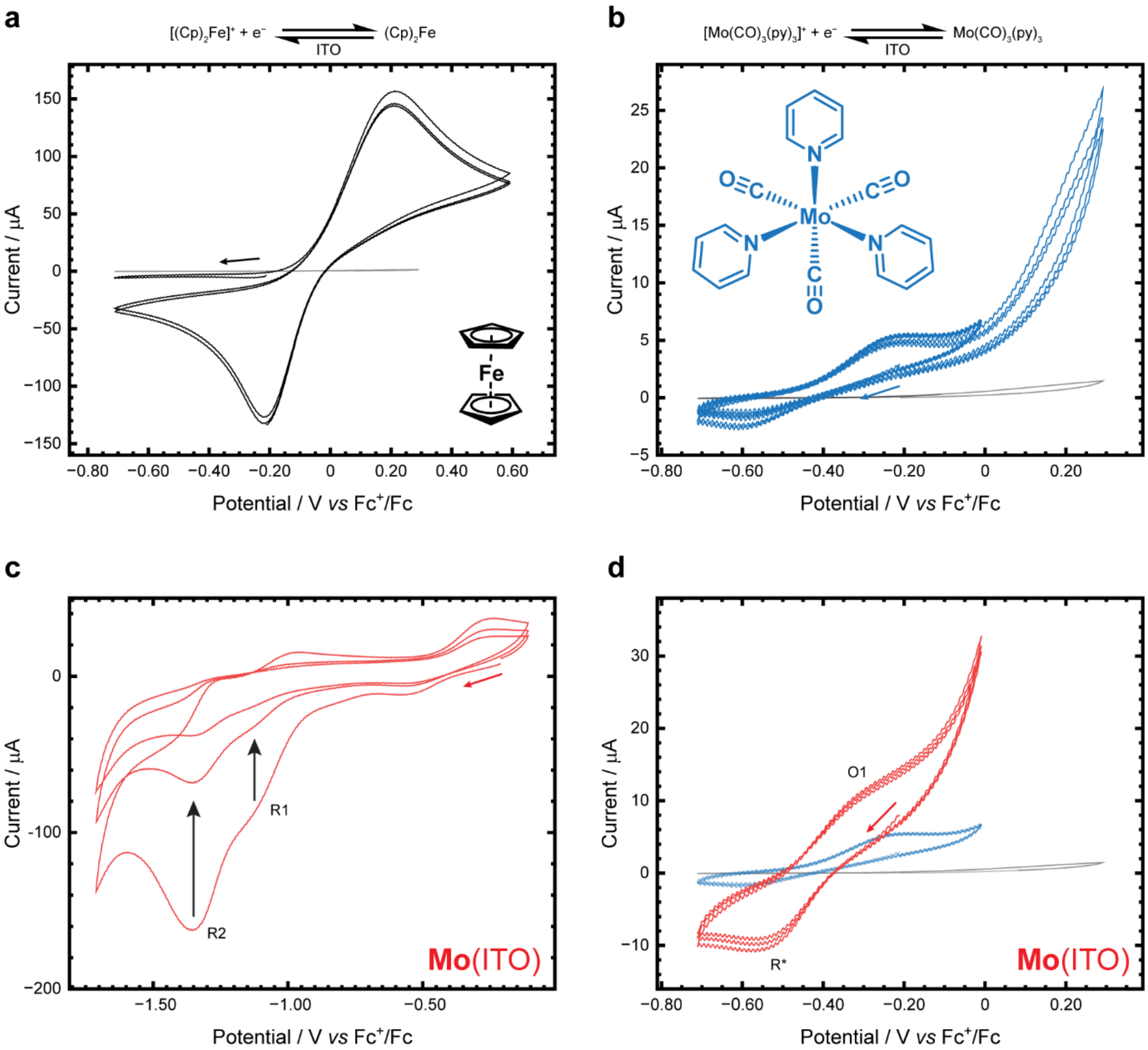

Fig. S23. Cyclic voltammograms related to the electrochemical studies of **Mo** (ITO). Voltammograms are shown for **a)** ferrocene, after the completion of the experiments, **b)** $Mo(CO)_3(py)_3$ cycling at two different potential ranges, **c) Mo** (ITO) cycling at negative potentials and **d)** non-normalized comparison of **Mo** (ITO) (red trace) and $Mo(CO)_3(py)_3$ (blue trace) and a blank ITO substrate (grey trace).

References

1 A. Pearson, E. Schoffers, *Organometallics* 1997, **16**, 5365-5367.

2 G. M. Sheldrick, *Acta Crystallogr A* 2015, **71**, 3–8.

3 G. M. Sheldrick, *Acta Crystallogr C Struct Chem* 2015, **71**, 3–8.

4 Rigaku Oxford Diffraction, AutoChem 5 software system in conjunction with Olex2 1.5-ac$^{\text{Neo}}$, Rigaku Corporation, Wroclaw, Poland, 2022.

5 S. Ito, F. J. White, E. Okunishi, Y. Aoyama, A. Yamano, H. Sato, J. D. Ferrara, M. Jasnowski, M. Meyer, *CrystEngComm* 2021, **23**, 8622–8630.

6 Rigaku Oxford Diffraction, CrysAlis$^{\text{Pro}}$ software system version 1.171.42.55a, Rigaku Corporation, Wroclaw, Poland, 2022.

7 N. Naudad, N. Lequeux, M. Nanot, J. Jove, T. Roisnel, *J. Solid State Chem.* 1998, **135**, 140-148.